XXVth IAP Colloquium (2009 July)

DAMPED AND SUB-DAMPED LYMAN-α ABSORBERS IN Z $>$ 4 QSOS

R. Guimarães[1], P. Petitjean[2] and A. Aghaee[3, 4]

Abstract. We present the results of a survey for damped (log$N$(H I) $>$ 20.3) and sub-damped Lyman-α systems (19.5 $<$ log$N$(H I) $<$ 20.3) at $z > 2.55$ along the lines of sight to 77 quasars with emission redshifts in the range $4 < z_{\rm em} < 6.3$. Intermediate resolution ($R \sim 4300$) spectra have been obtained with the Echellette Spectrograph and Imager (ESI) mounted on the Keck telescope. A total of 101 systems with log N(H I) > 19.5 are detected of which 40 systems are damped Lyman-α systems for an absorption length of $\Delta X = 378$. We study the evolution with redshift of the cosmological density of the neutral gas and find, consistently with previous studies at similar resolution, that $\Omega_{\rm DLA,HI}$ decreases at $z > 3.5$. The overall cosmological evolution of $\Omega_{\rm HI}$ shows a peak around this redshift. The H I column density distribution for log N (H I) ≥ 20.3 is fitted, consistently with previous surveys, with a single power-law of index $\alpha \sim$ -1.8$\pm$0.25. This power-law overpredicts data at the high-end and a second, much steeper, power-law (or a gamma function) is needed. There is a flattening of the function at lower H I column densities with an index of $\alpha \sim -1.4$ for the column density range log N (H I) = 19.5$-$21. The fraction of H I mass in sub-DLAs is of the order of 30%. The H I column density distribution does not evolve strongly from $z \sim 2.5$ to $z \sim 4.5$.

1 Introduction

The amount of neutral gas in the Universe is an important ingredient of galaxy formation scenarios because the neutral phase of the intergalactic medium is the reservoir for star-formation activity in the densest places of the universe where galaxies are to be formed. It is therefore very important to make a census of the mass in this phase and to determine its cosmological evolution (see e.g. Péroux et al. 2001).

The gas with highest H I column density is detected through damped Lyman-α absorptions in the spectra of remote quasars. Although damped wings are seen for column densities of the order of log N(H I) $\sim$ 18, the neutral phase corresponds to log N(H I) $\geq$ 19.5 (Viegas 1995). The column density defining the so-called damped Lyman-α (DLA) systems has been taken to be log N(H I) $\geq$ 20.3 because this corresponds to the critical mass surface density limit for star formation (Wolfe et al. 1986) but also because the equivalent width of the corresponding absorption is appropriate for a search of these systems in low resolution spectra. Therefore several definitions have been introduced. $\Omega_{\rm g}^{\rm DLA}$ is the mass density of baryons in DLA systems, defined arbitrarily as systems with log N(H I) $\geq$ 20.3. $\Omega_{\rm g}^{\rm HI}$ is the mass density of neutral hydrogen in all systems : DLAs, Lyman limit systems (LLS) and the Lyman-α forest. The mass density of H I in the Lyman-α forest is negligible because the slope of the H I column density distribution is larger than -2 (~ -1.5; the gas is highly ionized). It is more difficult to estimate the contribution of LLS as the column density of these systems is very difficult to derive directly because the Lyman-α line lies in the logarithmic regime of the curve of growth.

However, $\Omega_{\rm g}^{\rm HI}$ is not easily related to physical quantities as the LLS with log $N < 19.5$ are at least partly ionized when the ones with log $N > 19.5$ are not (see e.g. Meiring et al. 2008). On the contrary, as emphasized by Prochaska et al. (2005), hereafter PHW05, the mass density of the neutral phase, $\Omega_{\rm g}^{\rm neut}$, is a good indicator of the mass available for star-formation and should be prefered instead. Note that $\Omega_{\rm g}^{\rm neut}$ is not equal to $\Omega_{\rm g}^{\rm DLA}$.

[1] Universidade Estadual de Feira de Santana (UEFS), Av. Transnordestinam S/N, 40036-900, Feira de Santana, BA, Brasil

[2] Institut d'Astrophysique de Paris, UMR7095 CNRS, Université Pierre & Marie Curie, 98bis Boulevard Arago, 75014 Paris, France

[3] Department of Physics, Faculty of Science, University of Sistan and Baluchestan, 98135 Zahedan, Iran

[4] School of Astronomy and Astrophysics, Institute for Research in Fundamental Sciences (IPM), P .O. Box 19395-5531 Tehran, Iran

The column density limit at which the gas is mostly neutral cannot be defined precisely but should lie between log N(H I) = 19 and 19.5. In any case, a conservative position is to consider that all systems above 19.5 are neutral.

Whether or not the mass of the neutral gas in the systems with 19.5 < log N(H I) < 20.3 (the so-called sub-DLAs or super-LLS) is negligible has been the source of intense discussions in recent years. Note that these discussions are related to the mass in the *neutral* phase only. Indeed, it is known for long (e.g. Petitjean et al. 1993) that the *total* mass associated with the Lyman limit systems is larger than that of DLAs. Indeed the gas in the LLS phase is mostly ionized and located in extended halos whereas DLAs are located in dense and compact regions. Péroux et al. (2003), hereafter PMSI03, have been the first to consider the sub-DLAs as an important reservoir of neutral gas. They claim that at $z > 3.5$, DLAs could contain only 50% of the neutral gas, the rest being to be found in sub-DLAs. When correcting for this, they find that the comoving mass density shows no evidence for a decrease above $z = 2$. PHW05 questionned this estimate. They use the Sloan Digital Sky Survey to measure the mass density of predominantly neutral gas $\Omega_{\rm g}^{\rm neut}$. They find that DLAs contribute >80% of $\Omega_{\rm g}^{\rm neut}$ at all redshift. Uncertainties are very large however and the same authors estimate that the systems with log N(H I) > 19 (the super-LLS) could contribute 20-50 % of $\Omega_{\rm g}^{\rm HI}$. Therefore, the question of what is the contribution of super-LLS to $\Omega_{\rm g}^{\rm neut}$ is not settled yet.

In addition, the evolution of $\Omega_{\rm g}^{\rm neut}$ at the very high redshift, $z > 4$, is not known yet. PHW05 claim that there is no evolution of $\Omega_{\rm g}^{\rm DLA}$ for $z > 3.5$ but they caution the reader that results for $z > 4$ should be confirmed with higher resolution data. The reason is that the Lyman-α forest is so dense at these redshifts that it is very easy to misidentify a strong blend of lines with a DLA. Therefore $\Omega_{\rm g}^{\rm DLA}$ can be easily overestimated.

We present the result of a survey for DLAs and sub-DLAs at high redshift ($z > 2.55$) using intermediate resolution data. We identify a total of 101 systems with log N(H I) $\leq$ 19.5 of which 40 are DLAs over the redshift range $2.88 \leq z_{abs} \leq 4.74$ along 77 lines of sight towards quasars with emission redshift $4 \leq z_{\rm em} \leq 6.3$. The sample and data reduction are presented in Section 2. In Section 3 we describe the procedures used to select the absorption systems. Section 4 analyses statistical quantitities characterizing the evolution of DLAs and sub-DLAs and discusses the cosmological evolution of the neutral gas mass density. Conclusions are summarized in Section 5. We adopt $\Omega_{\rm m} = 0.3$, $\Omega_\Lambda = 0.7$ and $H_0 = 72$ km s^{-1}.

2 Observation and data reduction

Medium resolution (R $\sim$ 4300) spectra of all $z > 3$ quasars discovered in the course of the DPOSS survey (Digital Palomar Observatory Sky Survey; see, e.g., Kennefick et al. 1995, Djorgovski et al. 1999 and the complete listing of QSOs available at http://www.astro.caltech.edu/$\sim$george/z4.qsos) have been obtained with the Echellette Spectrograph and Imager (ESI, Sheinis et al 2002) mounted on the KECK II 10 m telescope. In total, 99 quasars have been observed.

The echelle mode allows to cover the full wavelength range from 3900 Å to 10900 Å in ten orders with $\sim$ 300 Å overlap between two adjacent orders. The instrument has a spectral dispersion of about 11.4 km s^{-1} pixel^{-1} and a pixel size ranging from 0.16 Å pixel^{-1} in the blue to 0.38 Å pixel^{-1} in the red. The 1 arcsec wide slit is projected onto 6.5 pixel resulting in a $R \sim$4300 spectral resolution.

Data reduction followed standard procedures using IRAF for 70% of the sample and the programme *makee* for the remaining. For the IRAF reduction, the procedure was as follows. The images were overscan corrected for the dual-amplifier mode. Each amplifier has a different baseline value and different gain which were corrected by using a script adapted from LRIS called *esibias*. Then all the images were bias subtracted and corrected for bad pixels. The images were divided by a normalized two-dimensional flat-field image to remove individual pixel sensitivity variations. The flat-field image was normalized by fitting its intensity along the dispersion direction using a high order polynomial fit, while setting all points outside the order aperture to unity. The echelle orders were traced using the spectrum of a bright star. Cosmic rays were removed from all two-dimensional images. For each exposure the quasar spectrum was optimally extracted and background subtracted. The task *apall* in the IRAF package *echelle* was used to do this. The CuAr lamps were individually extracted using the quasar's apertures. Lines were identified in the arc lamp spectra by using the task *ecidentify* and a polynomial was fitted to the line positions resulting in a dispersion solution with a mean RMS of 0.09 Å. The dispersion solution computed on the lamp was then assigned to the object spectra by using the task *dispcor*. Wavelengths and redshifts were computed in the heliocentric restframe. The different orders of the spectra were combined using the task *scombine* in the IRAF package. It is important to note that the signal-to-noise ratio drops sharply at

the edges of the orders. We have therefore carefully controlled this procedure to avoid any spurious feature.

The SNR per pixel was obtained in the regions of the Lyman-α forest that are free of absorption and the mean SNR value, averaged between the Lyman-α and Lyman-β QSO emission lines, was computed. We used only spectra with mean SNR ≥ 10. For simplicity, we excluded from our analysis broad absorption line (BAL) quasars. We therefore used 77 lines of sight out of the 99 available to us.

The continuum was automatically fitted (Aracil et al. 2004; Guimarães et al. 2007) and the spectra were normalized. We checked the normalization for all lines of sight and manually corrected for local defects especially in the vicinity of the Lyman-α emission lines and when the Lyman-α forest is strongly blended.

Metallicities measured for twelve $z > 3$ DLAs observed along five lines of sight of this sample have been published by Prochaska et al. (2003b); see also Prochaska et al. (2003a).

3 Identification of Damped and sub-Damped Lyman-α systems

We used an automatic version of the Voigt profile fitting routine VPFIT (Carswell et al. 1987) to decompose the Lyman-α forest of the spectra in individual components. As usual, we restricted our search outside of 3000 km s^{-1} from the QSO emission redshift. This is to avoid contamination of the study by proximate effects such as the presence of overdensities around quasars (e.g. Rollinde et al. 2005, Guimarães et al. 2007).

From this fit we could identify the candidates with log N(H I) − error ≥ 19.5. We then carefully inspected each of these candidates individually with special attention to the following characteristics of DLA absorption lines:

- the wavelength range over which the line is going to zero;
- the presence of damped wings;
- the identification of associated metal lines when possible.

The redshift of the H I absorptions was adjusted carefully using the associated metal absorption features and the final H I column density was then refitted using the high order lines in the Lyman series when Lyman series are covered by our spectrum and not blended with other lines. After applying the above criteria, 101 DLAs and sub-DLAs with log N(H I) ≥ 19.5 were confirmed.

The metal lines have been searched for using a search list of the strongest atomic transitions. The corresponding absorptions have been fitted using the package VPFIT.

4 Analysis

Using the procedure described in the previous Section, we detect 101 systems with log N (H I) ≥ 19.5, out of which 40 are DLAs. We use this sample to investigate the characteristics of the neutral phase over the redshift range $2.5 \leq z \leq 5$. We compare in Fig 1 the redshift sensitivity function of our survey with the redshift sensitivity function of previous surveys computed by PMSI03. Although the redshift path of our survey is much smaller than that of the SDSS survey (PHW05), it is at $z > 3.5$ similar to the surveys by Péroux et al. (2001, 2003). Note that our survey is homogeneous and at spectral resolution twice or more larger than previous surveys. The histogram of the H I column densities measured for the 101 DLAs and sub-DLAs is shown in Fig. 2. It is apparent that the histogram does not show the break usually seen below the completeness limit. We therefore are confident that we do not miss a large number of sub-DLAs down to the above limit.

To give a global overview of the survey, we plot in Fig. 3, log N(H I) versus $z_{\rm abs}$ for the 101 systems. In the same figure we show for comparison the data points from the Péroux et al. (2001) survey.

4.1 Column Density Distribution Function

The H I absorption system frequency distribution function is defined as:

$$f(N,X)dNdX = \frac{m_{\rm sys}}{\Delta N \times \sum_i^n \Delta X_{\rm i}} dNdX \qquad (4.1)$$

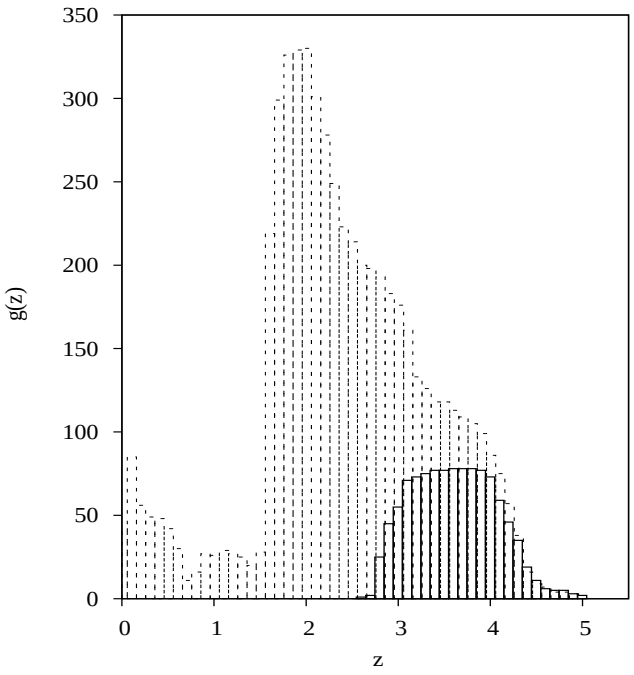

Fig. 1. Solid curve shows the redshift sensitivity function of our survey. Dashed curve shows the redshift sensitivity function of previous surveys computed by PMSI03.

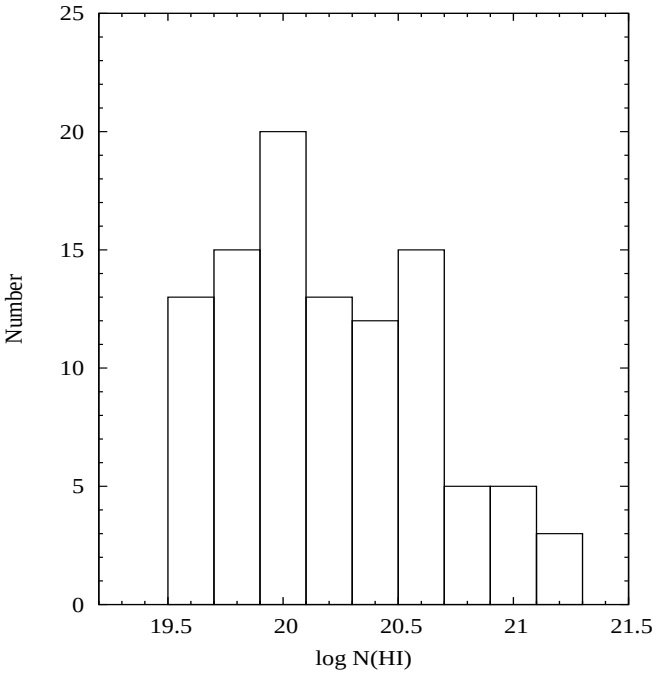

Fig. 2. Histogram of the H I column densities measured for the 101 DLAs and sub-DLAs with log N(H I) $\geq$ 19.5 detected in our survey.

where $m_{\rm sys}$ is the number of absorption systems with a column density comprized between $N - \Delta N/2$ and

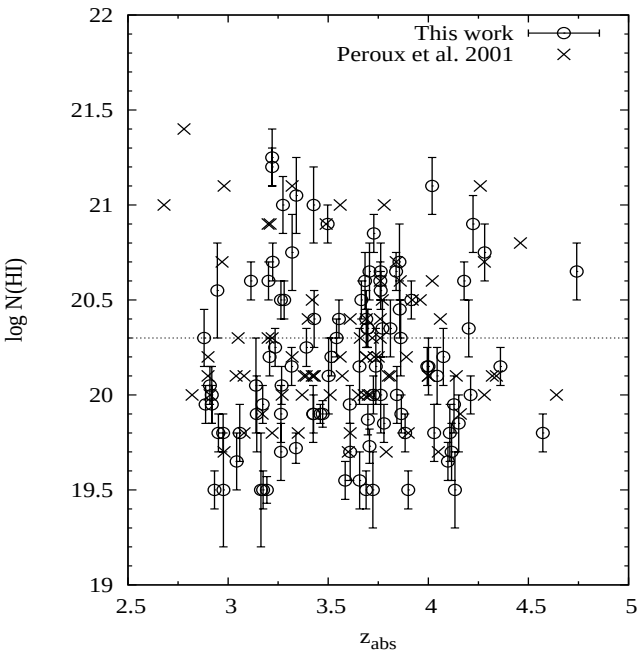

Fig. 3. The logarithm of the H I column density measured in our systems (circles) is plotted versus the redshift. The data points of Péroux et al. (2001) are shown for comparison with crosses.

$N + \Delta N/2$ and observed over an absorption distance interval of ΔX. The total absorption distance coverage, $\sum_i^n \Delta X_{\rm i}$, is computed over the whole sample of n QSO lines of sight. The absorption distance, X, is defined as

$$X(z) = \int_0^z (1+z)^2 E(z) dz \tag{4.2}$$

where $E(z) = [\Omega_{\rm M}(1+z)^3 + \Omega_\Delta]^{-1/2}$. For one line of sight, $\Delta X(z) = X(z_{\rm max}) - X(z_{\rm min})$, with $z_{\rm max}$ being the emission redshift minus 3000 km s^{-1} and $z_{\rm min}$ is the redshift of an H I Lyman-α line located at the position of the QSO Lyman-β emission line. In Figure 4 we show the function $f(N, X)$ obtained from our statistical sample over the redshift range $z = 2.55 - 5.03$ and for log N(H I) $\geq$ 19.5. It can be seen that there is no break at the low column density end, between log N(H I) = 19.5 and 20.6. This makes us confident that we are complete down to log N(H I) = 19.5. The vertical bars indicate 1σ errors. The horizontal bars indicate the bin sizes plotted at the mean column density for each bin. PHW05 results in the redshift range $z = 2.2 - 5.5$ and for log$N$(H I) $\geq$ 20.3 are overplotted in the same figure. Although our data points are consistent within about 1σ with those of PHW05, it seems that the overwhole shape of the function is flatter in our data. Note that we do not detect any system with log N(H I) > 21.25. Data points from Péroux et al. (2005), hereafter PDDKM05, are also overplotted. Our point at log$N$(H I) = 19.5 is consistent with theirs.

A power-law, a gamma function and/or a double power-law are usually used to fit the frequency distribution. It is apparent from Fig. 4 that a power-law (of the form $f(N, X) = K \times N^{-\alpha}$) fits the function nicely over the column density range 19.5 < log N(H I) < 21. The index of this power spectrum (see Table 1) is larger ($\alpha \sim$ -1.4) than what is found by PHW05 but over a smaller column density range log N(H I) > 20.3. The discrepancy is apparently due to the difference in the column density ranges considered by both studies. If we restrict our fit to the same range as PHW05 we find an index of $\alpha \sim$ -1.8$\pm$0.25 which is consistent with the results of PHW05. We note that PDDKM05 already mentioned that the small end of the column density distribution is flatter than $\alpha = -2$.

There is a large deficit of high column density systems in our survey compared to what would be expected from the single power-law fit. This has been noted before and discussed in detail by PHW05. A double power-law was used to fit our full sample with better result (see Table 1). However, the sharp break in the function

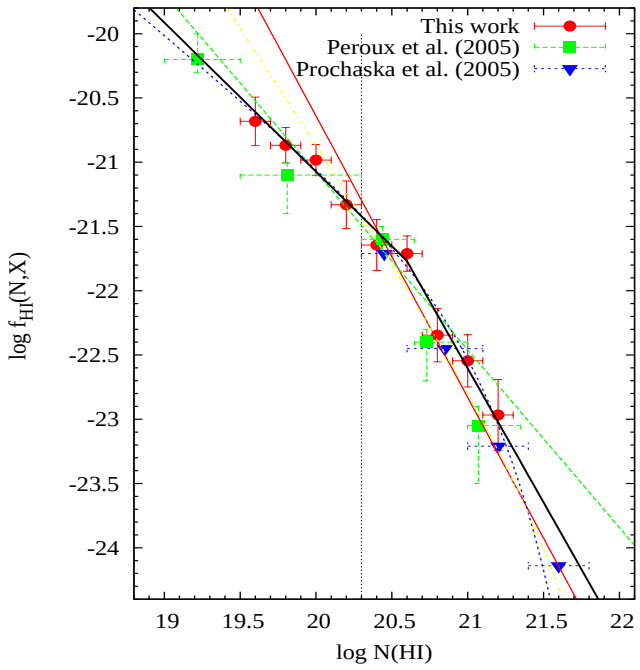

Fig. 4. Frequency distribution function over the redshift range $z = 2.55 - 5.03$. The dashed green, solide black and dotted blue lines are, respectively, a power-law, a double power-law and a gamma function fits to the data. The solid red and dash-dotted yellow lines are, respectively, a power-law and gamma function fits to the data obtained by PHW05.

at log N(H I) $\sim$ 21 suggests a gamma function of the form, $f(N,X) = K \times (\frac{N}{N_T})^{-\alpha} \times e^{\frac{-N}{N_T}}$ (Pei & Fall 1995) should better describe the data.

We have calculated the frequency distribution function, $f(N,X)$, in different redshift bins of equal distance path : 2.55−3.40; 3.40−3.83 and 3.83−5.03. Results are shown in Fig. 5. The functions are fitted as described above and fit results are given in Table 1. We find that the function do not evolve much with redshift. This is consistent with the finding by PHW05 that the global characteristics of the function are not changing much with time. There is however a tendancy for a flattening of the function which may indicate that the number of sub-DLAs relatively to other systems is larger at lower redshift. Although we do not think this is the case because we have used a conservative approach, part of this evolution at the highest redshift could possibly be a consequence of loosing the sub-DLAs in the strongly blended Lyman-α forest at $z > 4$. We note also a slight decrease of the number of systems with log N(H I) > 20.5 at the highest redshifts. This is consistent with the finding by PDDKM05 that the relative number of high column density DLAs decreases with redshift.

Another way to look at these variations is to compute the redshift evolution of the number of (sub)DLAs per unit path length. The observed density of systems is defined as

$$l_{\rm (sub)DLAs} = \int_{N_{\rm min}}^{N_{\rm max}} f(N,X) dN \tag{4.3}$$

Results obtained during the present survey together with those of PWH05 and PDDKM05 are plotted in Figure 6. The important feature of this plot is that the number density of DLAs peaks at $z \sim 3.5$. In addition, the ratio of the number of sub-DLAs to the number of DLAs is larger at redshift <3.5 compared to higher redshifts.

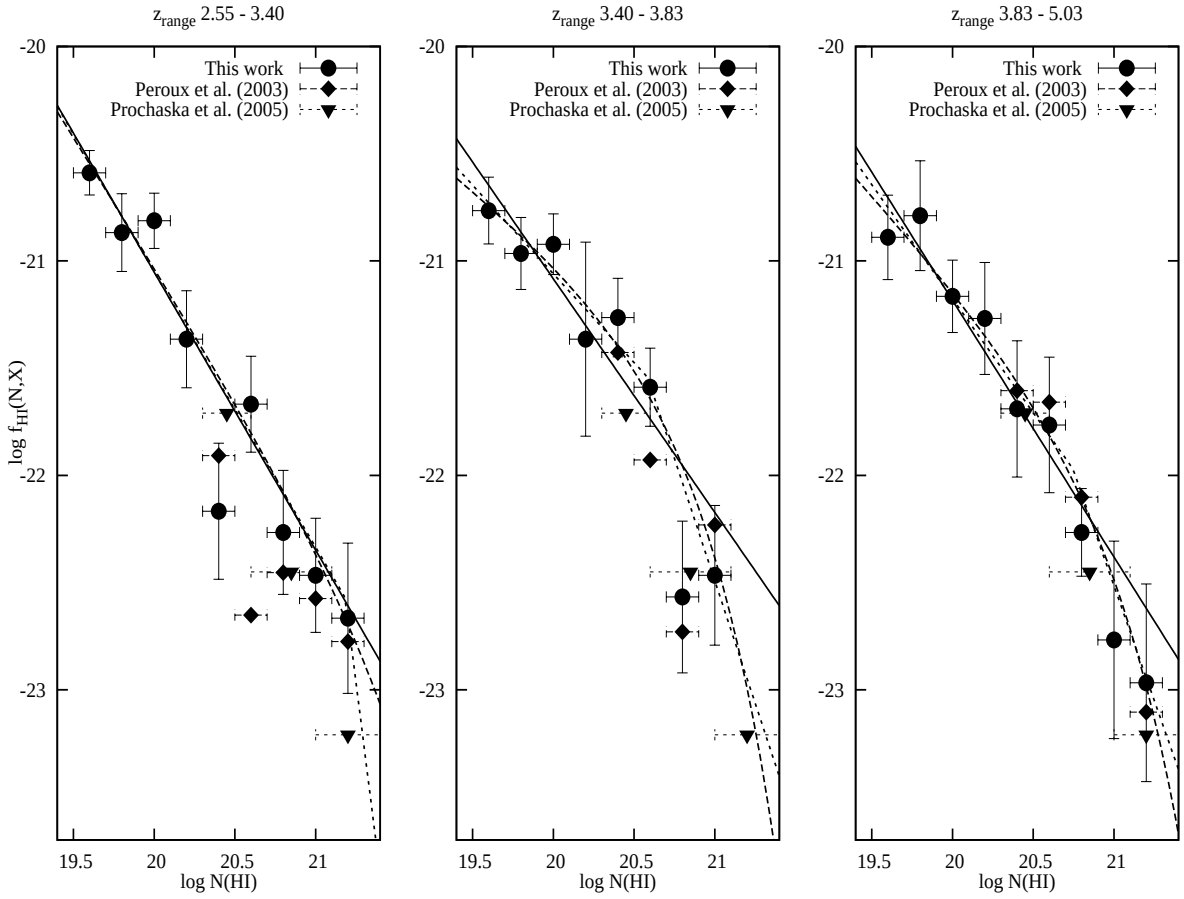

Fig. 5. H I frequency distribution, $f_{\rm HI}(N, X)$, in three redshifts bins: 2.55−3.40 (left), 3.40−3.83 (center), and 3.83−5.03 (right). Straight lines show best χ^2 fits of a power-law function to the binned data. The dashed curve is the same for a gamma function fit. and the dot-dashed curve for a double power-law fit.

4.2 Neutral hydrogen cosmological mass density, $\Omega_{\rm HI}$

The comoving mass density of neutral gas is given by

$$\Omega_{\rm HI}(z) = \frac{H_0}{c}\frac{\mu m_{\rm H}}{\rho_0}\frac{\Sigma_i N_i({\rm HI})}{\Delta X(z)} \tag{4.4}$$

where the density is in units of the current critical density ρ_0; $m_{\rm H}$ is the mass of the hydrogen atom, $\mu = 1.3$ is the mean molecular weight, ΔX the absorption length and the summation of column densities is done over all absorption systems detected in the survey. Results are shown in Fig. 7 and summarized in Table 2. The three redshift bins considered are defined so that the absorption length is equal in each bin. The different columns of Table 2 give, respectively, the redshift range, the mean redshift, the number of lines of sight involved, the number of DLAs and sub-DLAs detected over this redshift range, the absorption length (calculated using $z_{\rm min}$ and $z_{\rm max}$, the resulting H I cosmological densities for, respectively, DLAs only or both DLAs and sub-DLAs.

Results from PHW05 and PDDKM05 are also plotted on Figure 7. It can be seen that we confirm the decrease of $\Omega_{\rm HI}$ for $z > 3$ that was noticed by PDDKM05. The measurement from the SDSS in this redshift range is higher. However, our survey is of higher spectral resolution and should in principle be more reliable in this redshift range. It seems that the evolution of $\Omega_{\rm HI}$ is a steep increase from $z = 2$ to $z = 3$ and then a slightly flatter decrease up to $z = 5$. The inclusion of the sub-DLAs does not change this picture as sub-DLAs contribute to a maximum of about 30% to the total H I mass. The contribution by sub-DLAs is better seen in Fig. 8 where we plot the cumulative density versus the maximum H I column density considered. As noted

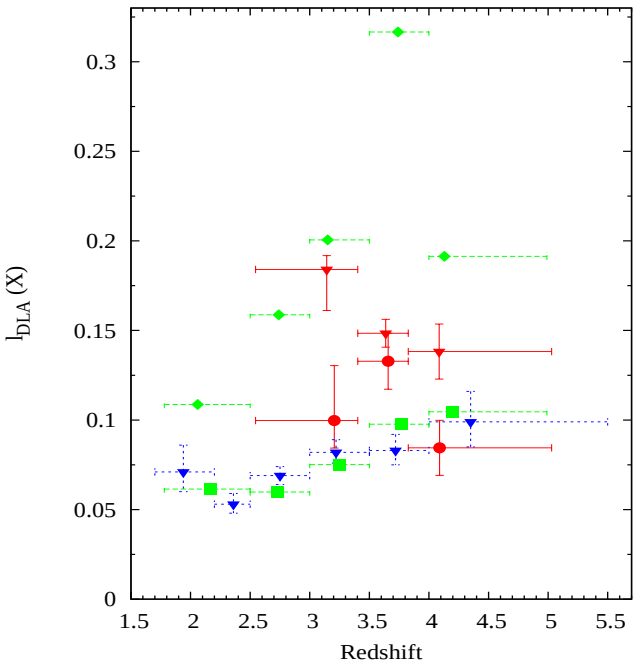

Fig. 6. Number density of absorbers vs. redshift. Red circles and inverse triangles are from this work for DLAs and sub-DLAs, respectively. The values obtained by PWH05 (blue inverse triangles) and PDDKM05 (green squares) for DLAs are overplotted. The green diamonds are the values obtained for log N(HI) > 19.0 by PDDKM05.

Table 1. Frequency distribution fitting parameters

Form	$z_{\rm range}$	log K	α	$logN_T$	β
Power-Law	[2.55 - 5.03]	6.59±2.12	−1.384±0.105	——-	——-
	[2.55 - 3.40]	5.55±2.88	−1.330±0.144	——-	——-
	[3.40 - 3.83]	4.03±2.01	−1.056±0.199	——-	——-
	[3.83 - 5.03]	4.38±2.39	−1.279±0.118	——-	——-
Double Power-Law	[2.55 - 5.03]	-21.78±0.31	−1.162±0.118	20.60±0.24	-2.07±0.51
	[2.55 - 3.40]	-22.64±1.25	−1.327±0.307	21.19±1.44	-5.98±2.07
	[3.40 - 3.83]	-21.28±0.19	−0.793±0.233	20.45±0.14	-2.49±0.74
	[3.83 - 5.03]	-21.63±0.25	−0.920±0.199	20.51±0.17	-2.10±0.44
Gamma	[2.55 - 5.03]	-21.95±0.36	−1.010±0.172	20.93±0.18	——-
	[2.55 - 3.40]	-22.53±1.54	−1.185±0.329	21.28±0.89	——-
	[3.40 - 3.83]	-20.96±0.28	−0.485±0.324	20.45±0.16	——-
	[3.83 - 5.03]	-21.80±0.35	−0.853±0.198	20.82±0.18	——-

already by numerous authors, the discrepancy of measurements at $z < 1.5$ is still a problem.

It can be also seen from the Figure 7 that $\Omega_{\rm HI}$ are lower than $\Omega_{stellar}$, the mass density in stars in local galaxies. We find for the ratio of the peak value of $\Omega_{\rm HI}$ to $\Omega_{stellar}$ for this work R $\sim$ 0.45. Previous surveys, PDDKM05 and PHW05, have found for the ratio 0.37 and 0.40 respectively.

5 Discussion

We have presented the results of a survey for damped and sub-damped Lyman-α systems (log$N$(H I) $\geq$ 19.5) at $z \geq 2.55$ along the lines of sight to 77 quasars with emission redshifts in the range $4 \geq z_{\rm em} \geq 6.3$. In total

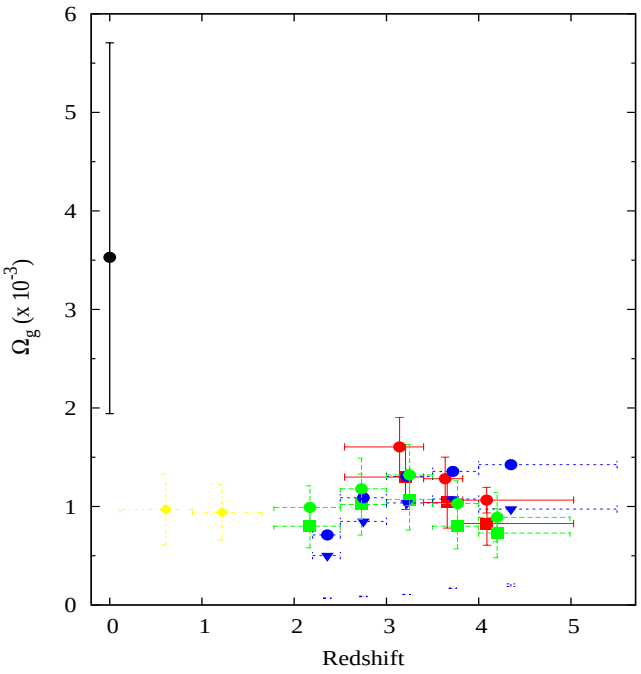

Fig. 7. Cosmological evolution of the H I mass density. For DLAs: red squares are the results of this work, green squares are from PDDKM05, blue inverse triangles from PHW05 and yelow diamonds from Rao et al. (2005). For sub-DLAs: red circles are this work (for systems with column densities $\geq$ 19.5), green circles obtained from PDDKM05 (for systems with column densities $\geq$ 19.0) and blue circles obtained from PHW05 (as determined from the single power-law fit to the LLS frequency distribution function). The black circle are the mass density in stars in local galaxies (Fukugita et al. 1998).

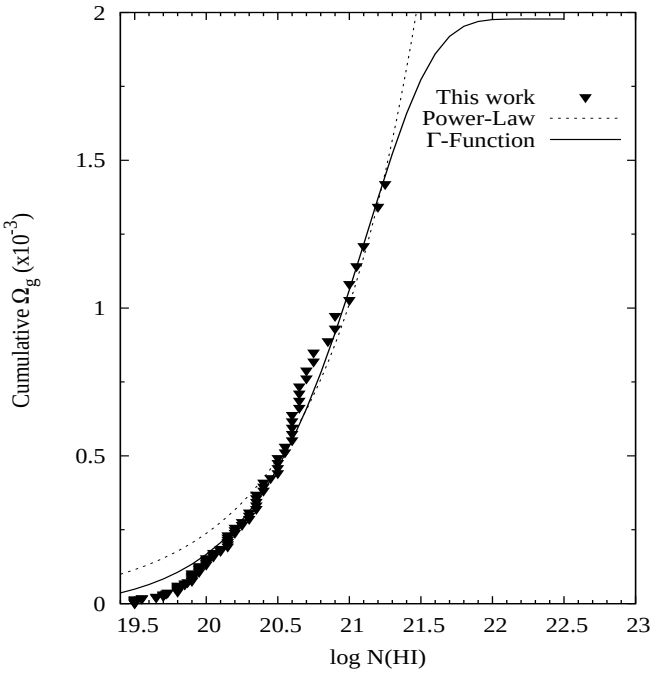

Fig. 8. $\Omega_{\rm HI}$ is plotted as a function of the maximum log N(H I) considered

Table 2. Absorption Distance Path - Data for Figure 7

$z_{\rm range}$	$< z >$	$N_{\rm QSO}$	$N_{\rm DLA}$	$N_{\rm subDLA}$	ΔX	$\Omega_{\rm DLA}$	$\Omega_{\rm DLA+subDLA}$
2.55 - 3.40	3.168	77	12	23	125.922	1.43 ± 0.33	1.71 ± 0.33
3.40 - 3.83	3.618	78	17	19	125.922	1.41 ± 0.26	1.65 ± 0.26
3.83 - 5.03	4.048	77	11	18	125.922	0.97 ± 0.22	1.21 ± 0.22

99 quasars were observed but 22 lines of sight were not used because of not enough SNR and/or because of the presence of broad absorption lines. Intermediate resolution ($R \sim 4300$) spectra have been obtained with the Echellette Spectrograph and Imager (ESI) mounted on the Keck telescope. The damped Lyman-α absorptions are identified on the basis of (i) the width of the saturated absorption, (ii) the presence of damped wings and (iii) the presence of metals at the corresponding redshift. The detection is run automatically but all lines are verified visually. A total of 101 systems with log N(H I) $\geq$ 19.5 are detected of which 40 systems are Damped Lyman-α systems (log N(H I) $\geq$ 20.3) for an absorption length of $\Delta X = 378$. Spectra are shown in Appendix.

PHW05 have derived from SDSS data that the cosmological density of the neutral gas increases strongly by a factor close to two from $z \sim 2$ to $z \sim 3.5$. Beyond this redshift, measurements are more difficult because the Lyman-α forest is dense. Our measurements should be more reliable because of better spectral resolution. We show, consistently with the findings of PDDKM05, that the cosmological density of the neutral gas decreases at $z > 3.5$. The overall cosmological evolution seems therefore to have a peak at this redshift.

We find that the H I column density distribution does not evolve strongly from $z \sim 2.5$ to $z \sim 4$. The one power-law fit in the range log N(H I) > 20.3 gives an index of $\alpha = -1.80 \pm 0.25$, consistent with previous determinations. However, we find that the fit over the column density range log N(H I) = 19.5$-$21 is quite flat ($\alpha \sim 1.4$). This probably indicates that the slope at the low-end is much flatter than -2. This power-law overpredicts data at the high-end and a second much steeper power-law (or a gamma function) is needed. The fraction of H I mass in sub-DLAs is of the order of 30%. Our data do not support the claim by PDDKM05 that the incidence of low column-density sytems is larger at high redshift. The number density of sub-DLAs seems to peak at $z \sim 3.5$ as well.

It is apparent that statistical errors are still large in our survey. It would be therefore of first importance to enlarge the sample of (sub)DLAs at high redshift. For this we need to go to fainter quasars however. The advent of X-shooter, a new generation spectrograph at the VLT with a spectral resolution of $R = 6700$ in the optical, should allow this to be done in a reasonable amount of observing time.

References

Aracil, B., Petitjean, P., Pichon, C., & Bergeron, J. 2004, AAP, 419, 811

Carswell, R. F., Webb, J. K., Baldwin, J. A., & Atwood, B. 1987, ApJ, 319, 709

Djorgovski, S. G., Odewahn, S. C., Gal, R. R., Brunner, R. J., & de Carvalho, R. R. 1999, in Weymann R. J., Storrie-Lombardi L. J., Sawicki M., Brunner R. J., eds, ASP Conf. Ser. Vol. 191, Photometric Redshifts and the Detection of High Redshift Galaxies. Astron. Soc. Pac., San Francisco, p. 179

Guimarães, R., Petitjean, P., Rollinde, E., de Carvalho, R. R., Djorgovski, S. G., Srianand, R., Aghaee, A., & Castro, S. 2007, MNRAS, 377, 657

Kennefick, J. D., Djorgovski, S. G., & de Carvalho, R. R. 1995, AJ, 110, 2553

Meiring, J. D., Kulkarni, V. P., Lauroesch, J. T., Péroux, C., Khare, P., York, D. G., & Crotts, A. P. S. 2008, MNRAS, 384, 1015

Pei, Y. C., & Fall, S. M. 1995, ApJ, 454, 69

Péroux, C., Storrie-Lombardi, L. J., McMahon, R. G., Irwin, M., & Hook, I. M. 2001, AJ, 121, 1799

Péroux, C., McMahon, R. G., Storrie-Lombardi, L. J., & Irwin, M. J. 2003, MNRAS, 346, 1103

Péroux, C., Dessauges-Zavadsky, M., D'Odorico, S., Sun Kim, T., & McMahon, R. G. 2005, MNRAS, 363, 479

Petitjean, P., Webb, J. K., Rauch, M., Carswell, R. F., & Lanzetta, K. 1993, MNRAS, 262, 499

Prochaska, J. X., Castro, S., & Djorgovski, S. G. 2003, APJs, 148, 317

Prochaska, J. X., Gawiser, E., Wolfe, A. M., Castro, S., & Djorgovski, S. G. 2003, APJl, 595, L9

Prochaska, J. X., Herbert-Fort, S., & Wolfe, A. M. 2005, APJ, 635, 123

Rao, S. M., Turnshek, D. A., & Nestor, D. B. 2006, APJ, 636, 610

Rollinde, E., Srianand, R., Theuns, T., Petitjean, P., & Chand, H. 2005, MNRAS, 361, 1015

Sheinis, A. I., Bolte, M., Epps, H. W., Kibrick, R. I., Miller, J. S., Radovan, M. V., Bigelow, B. C., & Sutin, B. M. 2002, PASP, 114, 851

Storrie-Lombardi, L. J., & Wolfe, A. M. 2000, APJ, 543, 552

Viegas, S. M. 1995, MNRAS, 276, 268

Wolfe, A. M., Turnshek, D. A., Smith, H. E., & Cohen, R. D. 1986, APJs, 61, 249